mathematics

MDPI

Article

# Predefined-Time Disturbance Observer-Based Nonsingular Sliding Mode Control with Prescribed Performance for Robotic Manipulators

**Shizhong Yang *, Yongyang Wang, Yi Yang and Guofa Sun**

School of Information and Control Engineering, Qingdao University of Technology, Qingdao 266520, China; wangyongyang@stu.qut.edu.cn (Y.W.); yangyi@stu.qut.edu.cn (Y.Y.); 901020150068@qut.edu.cn (G.S.)
* Correspondence: yszxlj@qut.edu.cn

**Abstract**

To achieve manipulator trajectory tracking under uncertainties and external disturbances, this study develops a prescribed performance nonsingular sliding mode control strategy. A new sufficient condition for predefined-time stability is established and proved. A predefined-time nonlinear disturbance observer is designed to estimate the lumped disturbance, and a prescribed performance function is introduced to confine the tracking error within predefined bounds. A predefined-time nonsingular sliding mode surface is constructed, while a saturation function and a hyperbolic tangent function are adopted to address singularity and chattering, respectively. Numerical simulations are conducted on a two-degree-of-freedom manipulator subject to 20% parametric uncertainties and time-varying external disturbances. The effectiveness of disturbance compensation is evaluated by comparing the control performance with and without observer compensation, and the proposed method is further compared with fixed-time and finite-time sliding mode controllers. Quantitative results show that, with observer compensation, the integral absolute error (IAE), integral squared error (ISE), and root mean square error (RMSE) are reduced by 71.63%, 12.95%, and 6.60% for Joint 1, and by 79.24%, 35.57%, and 19.55% for Joint 2, respectively. Moreover, compared with the fixed-time method, the proposed controller reduces the IAE by 54.3% for Joint 1 and 63.1% for Joint 2, while the corresponding reductions relative to the finite-time method are 89.0% and 93.3%, respectively. These results verify the effectiveness of the proposed scheme in disturbance rejection and tracking accuracy.

**Keywords:** predefined time control; disturbance observer; nonsingular sliding mode control; preset performance functions; trajectory tracking of manipulator

**MSC:** 93C73; 70B15; 93C85; 93D05

Check for updates

Academic Editor: Yiu Yin Raymond Lee

Received: 25 May 2026
Revised: 23 June 2026
Accepted: 26 June 2026
Published: 28 June 2026

**Copyright:** © 2026 by the authors. Licensee MDPI, Basel, Switzerland. This article is an open access article distributed under the terms and conditions of the Creative Commons Attribution (CC BY) license.

## 1. Introduction

Manipulator is the core equipment of industrial automation, which is widely used in many fields, such as precision machining, medical treatment, aerospace, and high-risk operations [1–3]. The system exhibits strong nonlinear and coupling properties and is prone to parameter fluctuations, unmodeled dynamics, load changes, and external disturbances in practical applications. These factors seriously restrict the tracking accuracy of traditional linear control methods (such as PID control) and may even lead to system instability. Consequently, the pursuit of high-performance trajectory tracking control strategies

that effectively suppress uncertainties and disturbances remains a long-standing research hotspot in manipulator control [4].

Sliding mode control [5] is widely used in manipulator control due to its invariance to matching interference, fast response, and simple implementation [6]. However, the traditional sliding mode control can only guarantee asymptotic stability, error exponential convergence, and theoretical convergence time is infinite [7]. By introducing nonlinear functions, terminal sliding mode control (TSMC) achieves finite-time convergence, thus improving the convergence rate [8,9]. However, the upper bound of convergence for finite time control depends on the initial state, and the convergence time may be much longer than expected when the initial deviation is large. To overcome this shortcoming, fixed-time (FT) theory was developed [10,11]; the upper bound of convergence time is a global constant that does not depend on the initial state, thereby greatly enhancing robustness against initial conditions. It has been successfully applied to trajectory tracking of a manipulator [12–14]. However, the convergence time of FT control is difficult to be directly specified by the designer, and its value is implicitly related to the controller parameters. To further address this issue, predefined-time (PT) control enables the convergence upper bound to be directly configured as an independent tuning parameter, thereby enhancing engineering operability [15]. Nie et al. Designed a nonsingular (NSMC) strategy based on a predefined time extended state observer [16], but there are still limitations: Refs. [17,18] only guaranteed the PT stability in the sliding phase and only the fixed time stability in the arrival phase; the method in references [19] may lead to singularity and infinite gain due to the introduction of a negative exponent. Although there are existing saturation function correction schemes [20,21], they can only guarantee stability in finite time or fixed time, and there is still a significant gap between the actual convergence time and the preset upper bound.

It is worth noting that the above research mainly focuses on the steady-state performance of the system, and the transient performance indicators such as overshoot and convergence rate are not fully considered. To solve this problem, Bechlioulis and Rovithakis innovatively proposed the concept of preset performance control (PPC) [22]. The core idea is to map the original control system to a new error coordinate system by introducing the preset performance function (PPF) to strictly restrict the tracking error within the user preset boundary and optimize the transient and steady-state behavior of the system. At present, PPC has been combined with a neural network [23], an extended state observer [24], and other methods to achieve a good control effect in uncertain systems.

The key to realizing PPC is to effectively estimate and compensate for uncertainties and external disturbances. Therefore, researchers have developed a variety of unknown dynamic estimation methods. Although neural networks [25–27] and fuzzy logic systems [28,29] can approximate unknown terms through nonlinear mapping, they are computationally expensive and thus cannot easily meet real-time requirements. In contrast, the nonlinear disturbance observer (NDO) [30,31] is favored for its simple structure and high estimation efficiency. However, traditional NDO is mostly based on asymptotic or finite time convergence, and the estimation speed depends on the gain selection, which has a long convergence time and is difficult to meet the high performance requirements. To overcome this issue, fixed-time nonlinear disturbance observers (FTNDO) have been developed and successfully applied to uncertain systems, including robotic manipulators, providing convergence properties independent of the initial state [32–34]. However, in most FTNDO designs, the convergence-time upper bound is still implicitly determined by observer parameters rather than being directly assignable by the designer. In the present work, since the disturbance estimation dynamics are embedded into a prescribed-performance and predefined-time sliding mode tracking framework, an observer with an explicitly

prescribable convergence-time bound is more suitable for coordinated time-scale design. Therefore, the development of a predefined-time nonlinear disturbance observer remains meaningful for the considered manipulator control problem.

Although prescribed-performance control and predefined-/fixed-time control have both been extensively investigated, and their combination has also been explored in recent manipulator-related studies [35,36], several issues still remain open. Existing methods often do not simultaneously address predefined-time lumped disturbance estimation, prescribed-performance-constrained tracking, singularity elimination in terminal sliding design, and chattering reduction within a unified manipulator control framework. Motivated by these observations, this paper develops an integrated predefined-time prescribed-performance tracking scheme with disturbance observation and smooth nonsingular sliding mode design.

To conclude, the key contributions of this study are as follows.

1. A new sufficient condition for PT stability is established, and rigorously verifies the correctness of the derived results. This condition provides a theoretical foundation for the unified stability analysis of the controller and observer, ensuring that the actual convergence time of the system meets the prescribed upper bound, thereby effectively improving the predictability of the convergence time.
2. A PTNDO is designed. The observer can accurately estimate the lumped disturbance composed of model uncertainties and external disturbances within a specified time, where the observation error is ultimately uniformly bounded, and the convergence time's upper bound can be preset.
3. A unified manipulator trajectory tracking control framework is constructed by integrating prescribed performance constraints, predefined-time nonsingular terminal sliding mode design, and smooth switching implementation. Within this framework, a saturation function is introduced to avoid singularity caused by negative-power terms, while a hyperbolic tangent function is employed to reduce chattering and improve torque smoothness. Compared with conventional finite-time and fixed-time sliding mode schemes, the proposed method provides prescribed tracking bounds together with improved disturbance rejection and smoother control inputs.

The remainder of this manuscript is organized as follows. In Section 2, the dynamic model of the two-degree-of-freedom robotic manipulator is established, along with relevant definitions and lemmas on predefined-time stability. Section 3 details the design of the PTNDO, the PPF, and the PTNTSMC. A comprehensive stability analysis is also provided. In Section 4, numerical simulation results are reported to validate the effectiveness of the proposed control scheme, including comparisons with finite-time and fixed-time sliding mode controllers. Finally, the conclusions of this paper are presented in Section 5.

## 2. Preliminaries and Problem Formulation

### 2.1. Preliminaries

Consider the nonlinear system

$$\dot{x} = f(x), \quad x(0) = x_0, \tag{1}$$

where $x \in \mathbb{R}^n$ denotes the system state, $f : \mathbb{R}^n \to \mathbb{R}^n$ is a nonlinear continuous function, and $f(0) = 0$.

**Definition 1** ([9])**.** *The origin of system (1) is said to be globally finite-time stable if it is globally asymptotically stable and every solution $x(t, x_0)$ converges to the equilibrium point in finite time*

*$T$. Specifically, for all $t \geq T(x_0)$, the solution satisfies $x(t, x_0) = 0$. Here, $T : \mathbb{R}^n \to \mathbb{R} \cup \{0\}$ is called the settling-time function.*

**Definition 2** ([13])**.** *System (1) is said to be fixed-time stable if it is globally finite-time stable and its settling-time function $T(x_0)$ has a uniform upper bound $T_{\max} > 0$ such that $T(x_0) \leq T_{\max}$ for all $x_0 \in \mathbb{R}^n$.*

**Definition 3** ([15])**.** *The equilibrium point of system (1) is said to be predefined-time stable if it is globally finite-time stable and its settling time $T(x_0)$ satisfies $T(x_0) \leq T_\delta$ for all $x_0 \in \mathbb{R}^n$, where $T_\delta > 0$ is called a predefined time constant.*

**Definition 4** ([18])**.** *The equilibrium point of system (1) is said to be practically predefined-time stable if, for any initial condition $x_0 \in \mathbb{R}^n$, there exist constants $\varepsilon > 0$ and a predefined time $T_\delta > 0$ such that $\|x(t)\| \leq \varepsilon, \quad \forall t \geq T_\delta$.*

**Theorem 1.** *Given system (1), assume there exists a Lyapunov function satisfying*

$$\dot{V} \leq -\frac{\pi}{\eta\zeta T_\delta}\left(V^{1-\frac{\eta}{2}} + \zeta^2 V^{1+\frac{\eta}{2}} + 2\zeta V\right), \tag{2}$$

*then system (1) is adjustable predefined-time stable, where $T_\delta > 0$ is the predefined time, $0 < \eta < 1$, and the parameter $\zeta > 0$ is an adjustable design parameter introduced in this paper; under the condition of Definition 3, it can be used to tune the actual convergence speed without changing the prescribed time $T_\delta$.*

**Proof.** Assume the settling time is $T_\Delta$ and $V(T_\Delta) = 0$. The initial state is $V(0) = V_0$. From (2) we obtain

$$\frac{\pi}{\eta\zeta T_\delta} dt \geq \frac{dV}{(V^{1-\frac{\eta}{2}} + \zeta^2 V^{1+\frac{\eta}{2}} + 2\zeta V)}$$

$$\frac{\pi}{\eta\zeta T_\delta}\int_0^{T_\Delta} dt \leq \int_0^{V_0} \frac{dV}{V^{1-\frac{\eta}{2}}(1 + \zeta^2 V^\eta + 2\zeta V^{\frac{\eta}{2}})}$$

$$\frac{\pi}{\eta\zeta T_\delta} T_\Delta \leq \frac{2}{\eta\zeta}\int_0^{V_0} \frac{d\zeta V^{\frac{\eta}{2}}}{(1 + \zeta V^{\frac{\eta}{2}})^2}, \tag{3}$$

then, using Young's inequality

$$\frac{\pi}{\eta\zeta T_\delta} T_\Delta \leq \frac{2}{\eta\zeta}\int_0^{V_0} \frac{d\zeta V^{\frac{\eta}{2}}}{1 + (\zeta V^{\frac{\eta}{2}})^2}$$

$$\frac{\pi}{\eta\zeta T_\delta} T_\Delta \leq \frac{2}{\eta\zeta}\arctan(\zeta V^{\frac{\eta}{2}})\Big|_0^{V_0} \leq \frac{\pi}{\eta\zeta}, \tag{4}$$

from the property $|\arctan(x)| < \frac{\pi}{2}$, we conclude

$$T_\Delta \leq T_\delta, \tag{5}$$

which shows that system (1) stabilizes within the predefined time. □

**Theorem 2.** *For system (1), if there exists a Lyapunov function $V(x)$ satisfying*

$$\dot{V} \leq -\frac{\pi}{\eta\zeta T_\delta}\left(V^{1-\frac{\eta}{2}} + \zeta^2 V^{1+\frac{\eta}{2}} + 2\zeta V\right) + \omega \tag{6}$$

*where $T_\delta > 0, 0 < \eta < 1, \zeta > 0, \omega > 0$, then the system is practically predefined-time stable, the convergence time is bounded by $\sqrt{2}T_\delta$, and the residual set of the solution is*

$$x \in \left\{ V(x) \leq \min\left\{ \left(\frac{2\omega\eta\zeta}{\pi}\right)^{\frac{2}{2-\eta}}, \left(\frac{2\omega\eta}{\zeta\pi}\right)^{\frac{2}{2+\eta}} \right\} \right\}. \tag{7}$$

**Remark 1.** *Compared with the classical predefined-time stability condition in [15] requiring $\dot{V} \leq -\frac{\pi}{\eta T_\delta}\left(V^{1-\frac{\eta}{2}} + V^{1+\frac{\eta}{2}}\right)$, Theorem 1 introduces an adjustable parameter $\zeta > 0$ and an additional cross term $2\zeta V$, yielding $\dot{V} \leq -\frac{\pi}{\eta\zeta T_\delta}\left(V^{1-\frac{\eta}{2}} + \zeta^2 V^{1+\frac{\eta}{2}} + 2\zeta V\right)$. The classical condition is recovered when $\zeta = 1$ and the cross term is omitted. As shown in Figure 1, it is observed that (a) the convergence time is independent of the initial value; (b) a smaller predefined time $T_\delta$ results in faster convergence; (c) the adjustable parameter $\zeta$ can tune the actual convergence rate without changing $T_\delta$; and (d) compared with the classical condition, the proposed condition yields a faster transient response while preserving the predefined-time bound. This condition is further used in the stability analysis of the disturbance observer (Theorem 3), the sliding dynamics on the designed sliding surface (Theorem 4), and the reaching dynamics under the proposed controller (Theorem 5).*

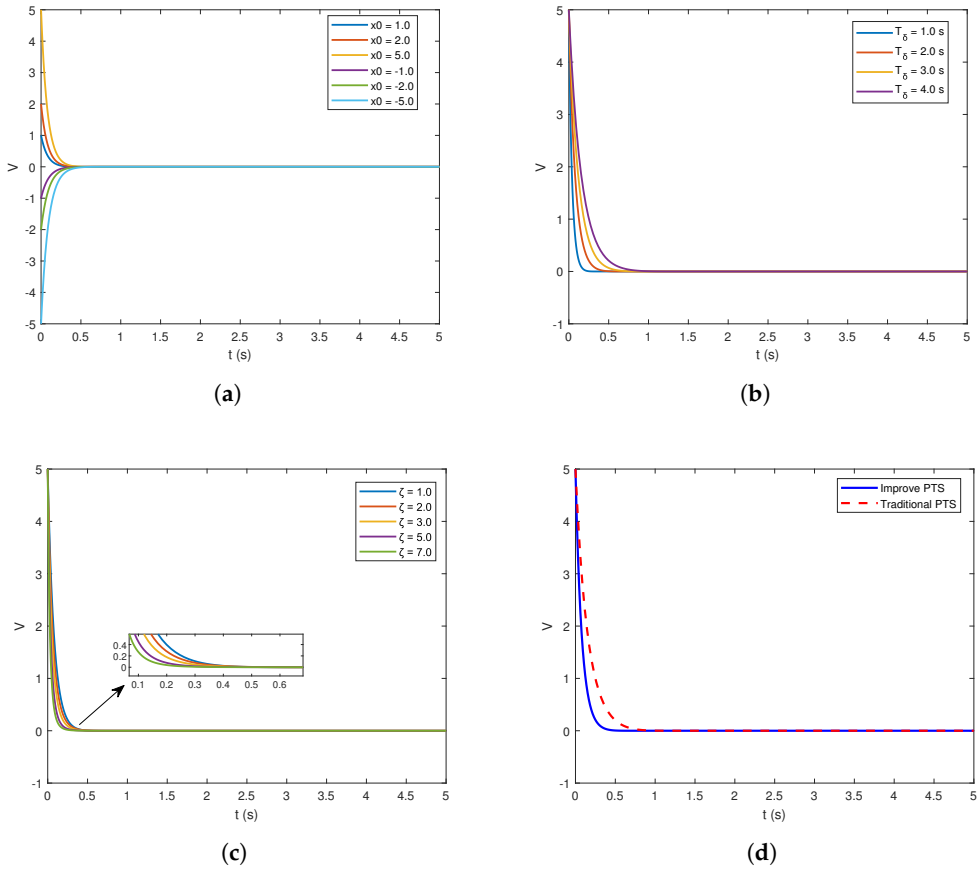


**Figure 1.** Effect of different parameters and comparison of predefined-time stability. (**a**) Effect of different initial values $x_0$, $\eta = 0.5, \zeta = 2, T_\delta = 1$; (**b**) Effect of predefined-time $T_\delta$, $\eta = 0.5, \zeta = 2$; (**c**) Effect of parameter $\zeta$, $\eta = 0.5, T_\delta = 1$; (**d**) Improved vs. traditional predefined-time stability, $x_0 = 5, \eta = 0.5, \zeta = 2, T_\delta = 2$

**Remark 2.** *For practical implementation, the predefined time $T_\delta$ should first be selected according to the task requirement while respecting actuator saturation limits, since a smaller $T_\delta$ generally leads to faster convergence but higher control peaks. Then, the adjustable parameter $\zeta > 0$ can be tuned according to the desired transient convergence speed, since it affects the actual convergence rate without changing the predefined-time bound $T_\delta$. The parameter $\eta \in (0,1)$ regulates the nonlinear convergence behavior and should be tuned together with $\zeta$ under actuator saturation constraints. As illustrated in Figure 1c, a larger $\zeta$ improves the transient response, while a smaller $\zeta$ leads to slower convergence. Therefore, $\eta$ and $\zeta$ should be jointly selected by balancing the desired convergence performance and actuator limits. If the resulting control peak approaches saturation, one may first reduce $\zeta$ and then retune $\eta$ accordingly to avoid overly aggressive transients.*

**Lemma 1.** *For $x_i \in \mathbb{R}$, $i = 1, 2, \ldots, n$, $0 < r_1 < 1$, $r_2 > 1$, the following inequalities hold*

$$\begin{aligned} \left(\sum_{i=1}^{n} x_i\right)^{r_1} &\leq \sum_{i=1}^{n} x_i^{r_1}, \\ \left(\sum_{i=1}^{n} x_i\right)^{r_2} &\leq n^{r_2-1} \sum_{i=1}^{n} x_i^{r_2}. \end{aligned} \tag{8}$$

**Lemma 2.** *Let $x$ be an $n$-dimensional vector with components $x_1, x_2, \ldots, x_n$. For any positive scalar $\kappa > 0$,*

$$\begin{aligned} \mathrm{sig}^{\kappa}(x) &= \left(|x_1|^{\kappa}\,\mathrm{sign}(x_1), \ldots, |x_n|^{\kappa}\,\mathrm{sign}(x_n)\right)^{\top} \in \mathbb{R}^n, \\ \mathrm{sign}(x) &= \left(\mathrm{sign}(x_1), \ldots, \mathrm{sign}(x_n)\right)^{\top} \in \mathbb{R}^n. \end{aligned} \tag{9}$$

### *2.2. Problem Description*

Consider a two-degree-of-freedom robotic manipulator. The dynamic model is derived using the Euler–Lagrange formulation

$$M(q)\ddot{q} + C(q,\dot{q})\dot{q} + G(q) + \tau_d = \tau, \tag{10}$$

where $q, \dot{q}, \ddot{q} \in \mathbb{R}^n$ are the joint position, velocity, and acceleration vectors, respectively. $M(q)$ is the symmetric positive definite inertia matrix, $C(q,\dot{q})$ is the Coriolis/centrifugal matrix, $G(q)$ is the gravity vector, $\tau$ is the applied torque, and $\tau_d$ is the bounded external disturbance. The dynamic model possesses the following properties.

**Property 1.** *$\dot{M}(q) - 2C(q,\dot{q})$ is a skew-symmetric matrix, satisfying $\forall x \in \mathbb{R}^n, x^T(\dot{M}(q) - 2C(q,\dot{q}))x = 0$.*

**Property 2.** *The inertia matrix $M(q)$ is symmetric positive definite; i.e., there exist positive numbers $m_1, m_2$ such that $m_1\|x\|^2 \leq x^T M(q) x \leq m_2\|x\|^2$.*

Due to uncertainties in dynamics and parameter identification, the actual model is decomposed into nominal and uncertain parts

$$\begin{cases} M(q) = M_0(q) + \Delta M(q) \\ C(q,\dot{q}) = C_0(q,\dot{q}) + \Delta C(q,\dot{q}) \\ G(q) = G_0(q) + \Delta G(q), \end{cases} \tag{11}$$

where $M_0, C_0, G_0$ denote the known nominal matrices, and $\Delta M, \Delta C, \Delta G$ represent modeling uncertainties.

Thus, the manipulator dynamics can be written as

$$M_0(q)\ddot{q} + C_0(q,\dot{q})\dot{q} + G_0(q) = \tau + d, \tag{12}$$

here, $d \in \mathbb{R}^n$ is the total disturbance, encompassing both model uncertainties and external disturbances. This disturbance $d$ is expressed as

$$d = -\Delta M(q)\ddot{q} - \Delta C(q,\dot{q})\dot{q} - \Delta G(q) - \tau_d. \tag{13}$$

**Assumption 1.** *The non-zero uncertainty $d$ satisfies the derivative condition $|\dot{d}| \leq \beta_d$, where $\beta_d$ is a known constant.*

**Remark 3.** *In practice, the bound $\beta_d$ in Assumption 1 may be unavailable a priori. A data-driven strategy can be used by reconstructing the lumped disturbance from representative simulation or experimental data, estimating its derivative after filtering, and selecting a conservative upper bound with a safety margin. Alternatively, $\beta_d$ may be replaced by an adaptive online estimate to relax the fixed-bound assumption. In this paper, Assumption 1 is retained for theoretical tractability, while the above strategies improve practical applicability.*

**Assumption 2.** *The desired joint angular position and velocity of the manipulator are known and continuous, with continuous second-order derivatives; the actual joint angular position and velocity are continuous and bounded.*

## 3. Controller Design

### *3.1. Predefined-Time Disturbance Observer Design*

For the purpose of estimating and compensating the total disturbance $d(t)$, which includes model uncertainties and external disturbances, let $\dot{q}(t) = v(t)$. Define the estimation error $\tilde{v} = v - \hat{v}$, with $\hat{v}$ being the estimate of $v$. The PTNDO is then given by

$$\begin{cases} \dot{\hat{v}} = M_0^{-1}\left(\tau - C_0 v - G_0 + C_0\tilde{v} + \hat{d}\right) \\ \hat{d} = \dfrac{\pi}{\eta\zeta T_d}\left(a_1 \operatorname{sig}^{1-\eta}(\tilde{v}) + a_2 \operatorname{sig}^{1+\eta}(\tilde{v}) + a_3\tilde{v}\right) \\ \qquad + \displaystyle\int_0^t \beta_d \cdot \operatorname{sign}(\tilde{v})\, \mathrm{d}s \end{cases} \tag{14}$$

where $0 < \eta < 1$, $\zeta > 0$, $T_d > 0$ is the predefined convergence time of the observation error, and the coefficients are $a_1 = \left(\frac{\|M_0\|}{2}\right)^{1-\frac{\eta}{2}}$, $a_2 = 2^{\frac{\eta}{2}}\zeta^2\left(\frac{\|M_0\|}{2}\right)^{1+\frac{\eta}{2}}$, $a_3 = 2\zeta\left(\frac{\|M_0\|}{2}\right)$.

**Theorem 3.** *Under Assumption 1, for the manipulator system (12), the proposed PTNDO (14) accurately estimates the lumped disturbance term that consists of external perturbations and model uncertainties, and this is done entirely within the predefined-time $T_d' = \sqrt{2}T_d$.*

**Proof.** Taking the derivative of $\tilde{v}$ and then applying left-multiplication by $M_0$, combined with the system dynamics and observer equations, we obtain

$$\begin{aligned} M_0\dot{\tilde{v}} &= M_0\dot{v} - M_0\dot{\hat{v}} \\ &= d - \hat{d} - C_0\tilde{v} \\ &= -\frac{\pi}{\eta\zeta T_d}\left(a_1 \operatorname{sig}^{1-\eta}(\tilde{v}) + a_2 \operatorname{sig}^{1+\eta}(\tilde{v}) + a_3\tilde{v}\right) + \sigma(t) - C_0\tilde{v} \end{aligned} \tag{15}$$

where $\dot{\sigma}(t) = \dot{d} - \beta_d \cdot \operatorname{sign}(\tilde{v})$.

Construct the Lyapunov function

$$V_d = \frac{1}{2}\tilde{v}^\top M_0 \tilde{v} \tag{16}$$

by differentiating $V_d$ with respect to time and invoking Property 1 along with Lemma 1, we obtain

$$\begin{aligned}
\dot{V}_d &= \tilde{v}^\top M_0 \dot{\tilde{v}} + \frac{1}{2}\tilde{v}^\top \dot{M}_0 \tilde{v} \\
&= \tilde{v}^\top \left( -\frac{\pi}{\eta \zeta T_d} \left( a_1 \operatorname{sig}^{1-\eta}(\tilde{v}) + a_2 \operatorname{sig}^{1+\eta}(\tilde{v}) + a_3 \tilde{v} \right) \right) \\
&\quad + \tilde{v}^\top \sigma - \tilde{v}^\top C_0 \tilde{v} + \frac{1}{2}\tilde{v}^\top \dot{M}_0 \tilde{v} \\
&= -\frac{\pi}{\eta \zeta T_d} \left( a_1 \sum_{i=1}^{2} |\tilde{v}_i|^{2-\eta} + a_2 \sum_{i=1}^{2} |\tilde{v}_i|^{2+\eta} + a_3 \tilde{v}^\top \tilde{v} \right) + \tilde{v}^\top \sigma \\
&\le -\frac{\pi}{\eta \zeta T_d} \left( a_1 \left( \|\tilde{v}\|^2 \right)^{1-\frac{\eta}{2}} + a_2 \cdot 2^{-\frac{\eta}{2}} \left( \|\tilde{v}\|^2 \right)^{1+\frac{\eta}{2}} + a_3 \|\tilde{v}\|^2 \right) + \tilde{v}^\top \sigma
\end{aligned} \tag{17}$$

from the matrix norm properties and Equation (16), we have

$$V_d \le \frac{1}{2}\|M_0\| \|\tilde{v}\|^2 \tag{18}$$

substituting $a_1, a_2, a_3$ into (17) and applying (18) leads to

$$\dot{V}_d \le -\frac{\pi}{\eta \zeta T_d} \left( V_d^{1-\frac{\eta}{2}} + \zeta^2 V_d^{1+\frac{\eta}{2}} + 2\zeta V_d \right) + \tilde{v}^\top \sigma, \tag{19}$$

according to (19), we investigate the boundedness of $\tilde{v}^\top \sigma$ by analyzing the sign of $\tilde{v}$. Because the initial values of the disturbances are unknown, we distinguish two different cases.

When $\tilde{v}(t) > 0$, the sign function yields $\operatorname{sign}(\tilde{v}) = 1$. According to Assumption 1, we have $\dot{\sigma}(t) \le |\dot{d}| - \beta_d \le 0$, which means $\tilde{v}(t)$ is decreasing. As soon as $\sigma(t) < 0$, $\tilde{v}$ and $\sigma(t)$ take opposite signs, leading to $\tilde{v}^\top \sigma(t) \le 0$.

When $\tilde{v}(t) < 0$, we obtain $\operatorname{sign}(\tilde{v}) = -1$. In the same manner, Assumption 1 yields $\dot{\sigma}(t) \ge |\dot{d}| - \beta_d \ge 0$, which implies that $\tilde{v}(t)$ rises. Once $\sigma(t) > 0$, $\tilde{v}$ and $\sigma(t)$ once more take opposite signs, leading again to $\tilde{v}^\top \sigma(t) \le 0$.

In either scenario, the inner product $\tilde{v}^\top \sigma(t)$ turns non-positive and, thus, possesses an upper bound. This upper bound is influenced by the initial values of the disturbance as well as the observer states, but it remains finite.

Thus, when $\tilde{v}^\top \sigma(t)$ is smaller than $\omega$ and at the same time $\tilde{v}^\top \sigma(t) \ge 0$ holds, we have that $\dot{V}_d$ satisfies

$$\dot{V}_d \le -\frac{\pi}{\eta \zeta T_d} \left( V_d^{1-\frac{\eta}{2}} + \zeta^2 V_d^{1+\frac{\eta}{2}} + 2\zeta V_d \right) + \omega \tag{20}$$

The above (20) formula shows that, via Theorem 1 and Theorem 2, once $t \ge \sqrt{2} T_d$, we have $\tilde{v} \to 0$. Consequently, the lumped disturbance error $\tilde{d}$ also approaches a small vicinity of zero within the predefined time $T_d' = \sqrt{2} T_d$. □

### 3.2. Prescribed Performance Function

As a core method in performance-constrained control, prescribed performance control provides an effective solution for the tracking error constraints of manipulator systems. By constructing a prescribed performance function and designing an error transformation mechanism, the tracking error can be strictly constrained within a predetermined boundary.

This strategy not only ensures system stability but also optimizes the dynamic response, significantly improving transient performance.

To guarantee that the tracking error approaches a small vicinity of zero within a predefined time, thus realizing stable following of the target trajectory, define the tracking error $e(t) \in \mathbb{R}^n$ as

$$e = q - q_d, \tag{21}$$

where $e = [e_1, e_2, \ldots, e_r]^\top$, and $q_d$ and $q$ denote the desired and actual joint angles of the manipulator, respectively. The tracking error is considered to converge with prescribed performance when it remains strictly within the prescribed region given as follows

$$-\rho_1 \lambda(t) < e(t) < \rho_2 \lambda(t) \tag{22}$$

where $0 < \rho_1 = \mathrm{diag}(\rho_{11}, \ldots, \rho_{1r}) \leq 1$, $0 < \rho_2 = \mathrm{diag}(\rho_{21}, \ldots, \rho_{2r}) \leq 1$ are given constants. $\lambda(t)$ is called the performance function, defined as

$$\lambda(t) = (\lambda_0 - \lambda_\infty) \exp^{(-\kappa t)} + \lambda_\infty, \tag{23}$$

with $\kappa > 0$, $\lambda_0 > 0$, $\lambda_\infty = \lim_{t\to\infty} \lambda(t) > 0$. By design, $\lambda(t)$ is positive, smooth, bounded, and monotonically decreasing.

**Remark 4.** *The parameter $\kappa$ in the prescribed performance function $\lambda(t)$ determines how fast the prescribed performance boundary shrinks from $\lambda_0$ to $\lambda_\infty$. If a desired boundary value $\lambda(t_s)$ is specified at a given time instant $t_s > 0$, then $\kappa$ can be selected as $\kappa = -\frac{1}{t_s} \ln\left(\frac{\lambda(t_s)-\lambda_\infty}{\lambda_0-\lambda_\infty}\right)$, so that a smaller $t_s$ requires a larger $\kappa$ and hence a faster boundary decay. However, $\kappa$ should be coordinated with the predefined-time parameters of the observer and controller. An excessively large $\kappa$ may cause the performance boundary to shrink much faster than the predefined-time convergence process of the sliding-mode dynamics, so that the transformed error increases rapidly during the transient stage and larger control peaks may arise. On the other hand, an overly small $\kappa$ weakens the prescribed-performance effect.*

Considering constraint (22), to handle the tracking error constraints in the original manipulator system, the following error transformation is introduced

$$z_{1i} = \Upsilon\left(\frac{e_i}{\lambda_i(t)}\right) = \left[1 - \varphi\left(\frac{e_i}{\lambda_i(t)}\right)\right] \frac{\frac{e_i}{\lambda_i(t)}}{\rho_{1i} + \frac{e_i}{\lambda_i(t)}} + \varphi\left(\frac{e_i}{\lambda_i(t)}\right) \frac{\frac{e_i}{\lambda_i(t)}}{\rho_{2i} - \frac{e_i}{\lambda_i(t)}}, \tag{24}$$

where

$$\varphi\left(\frac{e_i}{\lambda_i(t)}\right) = \begin{cases} 1, & \frac{e_i}{\lambda_i(t)} \geq 0, \\ 0, & \frac{e_i}{\lambda_i(t)} < 0, \end{cases} \tag{25}$$

thus,

$$z_{1i} = (1-\varphi) \frac{\frac{e_i}{\lambda_i(t)}}{\rho_{1i} + \frac{e_i}{\lambda_i(t)}} + \varphi \frac{\frac{e_i}{\lambda_i(t)}}{\rho_{2i} - \frac{e_i}{\lambda_i(t)}}. \tag{26}$$

Differentiating $z_{1i}$ gives

$$\dot{z}_{1i} = P_i(\dot{e}_i + H_i e_i), \tag{27}$$

where the parameters satisfy $P_i = (1-\varphi)\left[1 + e_i/(\rho_{1i}\lambda_i(t))\right]^{-2} + \varphi\left[1 - e_i/(\rho_{2i}\lambda_i(t))\right]^{-2} > 0$, $H_i = -\dot{\lambda}_i(t)/\lambda_i(t)$. Define the state vector $z_1 = [z_{11}, \ldots, z_{1r}]^\top$; then the transformed system can be expressed as $\dot{z}_1 = z_2$, where

$$z_2 = P(\dot{e} + He), \tag{28}$$

with $P = \mathrm{diag}(P_1, \ldots, P_r)$, $H = \mathrm{diag}\left(-\dot{\lambda}_1(t)/\lambda_1(t), \ldots, -\dot{\lambda}_r(t)/\lambda_r(t)\right)$. Differentiating $z_2$ yields

$$\begin{cases} \dot{z}_1 = z_2, \\ \dot{z}_2 = P(\ddot{e} + \dot{H}e + H\dot{e}) + \dot{P}(\dot{e} + He). \end{cases} \tag{29}$$

Through the above transformation, the tracking error is transformed, and the corresponding prescribed performance controller is designed accordingly.

### 3.3. Predefined-Time Nonsingular Terminal Sliding Mode Surface Design

To achieve convergence of the tracking errors $z_1, z_2$ within a predefined time, a novel predefined-time sliding mode surface is designed as follows

$$s = z_2 + b_1 \,\mathrm{sig}^{1-\eta_1}(z_1) + b_2 \,\mathrm{sig}^{1+\eta_1}(z_1) + b_3 z_1, \tag{30}$$

where $s = [s_1, s_2]^\top$, parameters satisfy $1 > \eta_1 > 0$, $\zeta_1 > 0$, $T_{\delta 1} > 0$, and the coefficients are defined as $b_1 = \left(\frac{1}{2}\right)^{1-\frac{\eta_1}{2}} \frac{\pi}{\eta_1 \zeta_1 T_{\delta 1}}$, $b_2 = \frac{1}{2} \cdot \frac{\zeta_1 \pi}{\eta_1 T_{\delta 1}}$, $b_3 = \frac{\pi}{\eta_1 T_{\delta 1}}$.

**Theorem 4.** *For the designed sliding mode surface (30), when the system state reaches the sliding surface and remains in the sliding phase, the tracking error will converge to a small neighborhood near the origin within the predefined time $T_{\delta 1}$.*

**Proof.** When the system is on the sliding surface, $s = 0$, leading to

$$\dot{z}_1 = -b_1 \,\mathrm{sig}^{1-\eta_1}(z_1) - b_2 \,\mathrm{sig}^{1+\eta_1}(z_1) - b_3 z_1. \tag{31}$$

choose the positive definite Lyapunov function $V_1 = \frac{1}{2} z_1^\top z_1$. Differentiating and substituting (31) gives

$$\begin{aligned} \dot{V}_1 &= z_1^\top \dot{z}_1 \\ &= z_1^\top \left(-b_1 \,\mathrm{sig}^{1-\eta_1}(z_1) - b_2 \,\mathrm{sig}^{1+\eta_1}(z_1) - b_3 z_1\right) \\ &= -b_1 \sum_{i=1}^{2} |z_{1i}|^{2-\eta_1} - b_2 \sum_{i=1}^{2} |z_{1i}|^{2+\eta_1} - b_3 z_1^\top z_1 \\ &\le -b_1 \left(\|z_1\|^2\right)^{1-\frac{\eta_1}{2}} - b_2 \cdot 2^{-\frac{\eta_1}{2}} \left(\|z_1\|^2\right)^{1+\frac{\eta_1}{2}} - b_3 \|z_1\|^2 \\ &\le -\frac{\pi}{\eta_1 \zeta_1 T_{\delta 1}} \left(V_1^{1-\frac{\eta_1}{2}} + \zeta_1^2 V_1^{1+\frac{\eta_1}{2}} + 2\zeta_1 V_1\right). \end{aligned} \tag{32}$$

according to Theorem 1, from (32) we conclude that after reaching the sliding surface, the system state converges to zero within the predefined time $T_{\delta 1}$. □

Differentiating the sliding surface (30) and substituting the system dynamics gives

$$\begin{aligned} \dot{s} = {} & P\left(M_0^{-1}\tau - M_0^{-1}(G_0 + C_0\dot{q}) + M_0^{-1}\tau + d - \ddot{q}_d + \dot{H}e + H\dot{e}\right) + \dot{P}(\dot{e} + He) + b_3 z_2 \\ & + b_1(1-\eta_1)|z_1|^{-\eta_1} z_2 + b_2(1+\eta_1)|z_1|^{\eta_1} z_2, \end{aligned} \tag{33}$$

based on sliding mode control theory, the condition $\dot{s} = 0$ leads to the equivalent control law.

$$\tau_{eq} = M_0\left(\ddot{q}_d - \dot{H}e - H\dot{e} - \hat{d}\right) - G_0 - C_0\dot{q} - M_0P^{-1}\Big[b_1(1-\eta_1)|z_1|^{-\eta_1}\dot{z}_1 + b_3\dot{z}_1 + b_2(1+\eta_1)|z_1|^{\eta_1}\dot{z}_1 + \dot{P}(\dot{e}+He)\Big], \tag{34}$$

note that the term containing $|z_1|^{-\eta_1}\dot{z}_1$ introduces a singularity when $z_{1i} = 0$ and $\dot{z}_{1i} \neq 0$, causing $|z_1|^{-\eta_1}\dot{z}_1$ to become very large, as shown in Figure 2, and is practically infeasible. To address this, inspired by the literature, a saturation function is introduced to resolve the singularity issue, expressed as

$$\mathrm{sat}(\Upsilon, \beta) = \begin{cases} \Upsilon, & |\Upsilon| \leq \beta \\ \beta\,\mathrm{sign}(\Upsilon), & |\Upsilon| > \beta \end{cases} \tag{35}$$

where $\beta > 0$ is a design constant. After introducing the saturation function, the equivalent control law is modified as

$$\tau_{eq} = M_0\left(\ddot{q}_d - \dot{H}e - H\dot{e} - \hat{d}\right) - G_0 - C_0\dot{q} - M_0P^{-1}\big[\mathrm{sat}\big(b_1(1-\eta_1)|z_1|^{-\eta_1}\dot{z}_1, \beta\big) + b_3\dot{z}_1 + b_2(1+\eta_1)|z_1|^{\eta_1}\dot{z}_2 + \dot{P}(\dot{e}+He)\big]. \tag{36}$$

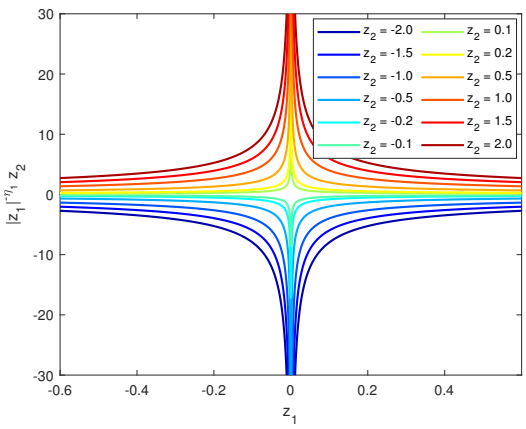


**Figure 2.** Singular term $|z_1|^{-\eta_1}\dot{z}_1$ versus $z_1$.

Further design the switching control term as

$$\tau_{sw} = -M_0P^{-1}\Big[c_1|s|^{1-\eta_2}\,\mathrm{sign}(s) + c_2|s|^{1+\eta_2}\,\mathrm{sign}(s) + K\tanh(\theta s) + c_3 s\Big] \tag{37}$$

where $K > 0$ is the control gain, satisfying $K > \tilde{d}$ for robustness; $T_{\delta 2} > 0$ is a predefined parameter, $\eta_2, \zeta_2 > 0$ are convergence accuracy parameters. For simplicity, define the coefficients $c_1 = \pi(1/2)^{1-\eta_2/2}/(\eta_2\zeta_2T_{\delta 2})$, $c_2 = \pi\zeta_2/(2\eta_2T_{\delta 2})$, $c_3 = \pi/(\eta_2T_{\delta 2})$. To attenuate chattering caused by the discontinuous switching gain $K\,\mathrm{sign}(s)$, the hyperbolic tangent function $\tanh(\theta s) = \frac{e^{\theta s}-e^{-\theta s}}{e^{\theta s}+e^{-\theta s}}$ is used to replace $\mathrm{sign}(s)$, where $\theta > 0$ is a design parameter. Finally, the manipulator control law is designed as $\tau = \tau_{eq} + \tau_{sw}$.

**Theorem 5.** *For the control system (12), if the controller (36) and (37) is applied, then the sliding variable $s$ will converge to zero within the predefined time $T_{\delta 2}$.*

**Proof.** Choose the positive definite Lyapunov function

$$V_2 = \frac{1}{2}s^{\top}s, \tag{38}$$

differentiating gives

$$\dot{V}_2 = s^\top \dot{s}. \tag{39}$$

substituting the system dynamics and the derivative of the sliding surface, we obtain

$$\dot{V}_2 = s^\top \Big( \dot{z}_2 + b_1(1-\eta_1)|z_1|^{-\eta_1}\dot{z}_1 + b_3\dot{z}_1 + b_2(1+\eta_1)|z_1|^{\eta_1}\dot{z}_1 \Big). \tag{40}$$

expanding further, using the transformation relation $z_2 = P(\dot{e} + He)$ and the system dynamics, we have

$$\begin{aligned} \dot{V}_2 = s^\top \Big[ & P\big(M_0^{-1}\tau - M_0^{-1}(G_0 + C_0\dot{q}) + d - \ddot{q}_d + \dot{H}e + H\dot{e}\big) + \dot{P}(\dot{e} + He) + b_3 z_2 \\ & + b_1(1-\eta_1)|z_1|^{-\eta_1}\dot{z}_1 + b_2(1+\eta_1)|z_1|^{\eta_1}\dot{z}_1 \Big]. \end{aligned} \tag{41}$$

To facilitate analysis, partition the state space $(z_1, z_2)$ into two regions

$$\psi_1 = \big\{ (z_1, e_2) : b_1(1-\eta_1)|e_1|^{-\eta_1} z_2 \le \beta \big\}, \tag{42}$$

$$\psi_2 = \big\{ (z_1, e_2) : b_1(1-\eta_1)|e_1|^{-\eta_1} z_2 > \beta \big\}. \tag{43}$$

when $(z_1, z_2) \in \psi_1$, we have

$$\mathrm{sat}\big(b_1(1-\eta_1)|z_1|^{-\eta_1}\dot{z}_1, \beta\big) = b_1(1-\eta_1)|z_1|^{-\eta_1}\dot{z}_1 \tag{44}$$

substituting the controller (36) and (37) into (41) yields

$$\begin{aligned} \dot{V}_2 &= s^\top \Big( -c_1 \,\mathrm{sig}^{1-\eta_2}(s) - c_2 \,\mathrm{sig}^{1+\eta_2}(s) - c_3 s - K\tanh(\theta s) + d - \hat{d} \Big) \\ &= -s^\top \big( c_1 \,\mathrm{sig}^{1-\eta_2}(s) + c_2 \,\mathrm{sig}^{1+\eta_2}(s) + c_3 s + K\tanh(\theta s) - \tilde{d} \big). \end{aligned} \tag{45}$$

Since $K > |\tilde{d}|$ and $s_i \tanh(\theta s_i) \ge |s_i| - 0.2785/\theta$, by virtue of Lemma.1 and matrix norm properties, we obtain

$$\dot{V}_2 \le -c_1 \sum_{i=1}^{2} |s_i|^{2-\eta_2} - c_2 \sum_{i=1}^{2} |s_i|^{2+\eta_2} - c_3 s^\top s + \varpi, \tag{46}$$

where $\varpi = 0.557K/\theta$ is a bounded constant. Further applying norm inequalities yields

$$\begin{aligned} \dot{V}_2 &\le -c_1 \big(\|s\|^2\big)^{1-\frac{\eta_2}{2}} - c_2 \cdot 2^{-\frac{\eta_2}{2}} \big(\|s\|^2\big)^{1+\frac{\eta_2}{2}} - c_3\|s\|^2 + \varpi \\ &\le -\frac{\pi}{\eta_2 \zeta_2 T_{\delta 2}} \left( V_2^{1-\frac{\eta_2}{2}} + \zeta_2^2 V_2^{1+\frac{\eta_2}{2}} + 2\zeta_2 V_2 \right) + \varpi. \end{aligned} \tag{47}$$

according to Theorem 2, from (47) it follows that when $(z_1, z_2) \in \psi_1$, the sliding variable $s$ converges to a small neighborhood of the origin within the predefined time $T'_{\delta 2} \le \sqrt{2}T_{\delta 2}$.

When the state $(z_1, z_2)$ lies in region $\psi_2$, two cases exist: $z_2(t) > 0$ or $z_2(t) < 0$. In this case, the solution for $z_1$ is

$$z_1(t) = z_1(0) + \int_0^t z_2(\tau)\,\mathrm{d}\tau. \tag{48}$$

Since $z_1(t)$ and $z_2(t)$ have the same monotonicity, when $z_2(t) > 0$, $z_1(t)$ increases monotonically until it reaches or crosses the boundary between $\psi_1$ and $\psi_2$; when $z_2(t) < 0$, $z_1(t)$ decreases monotonically and will also reach the boundary. Therefore, the error state $(z_1, z_2)$ necessarily transitions from region $\psi_2$ to region $\psi_1$ and does not stay in $\psi_2$

indefinitely. The existence of region $\psi_2$ does not affect the stability analysis; once the system enters $\psi_1$, the condition for predefined-time stability stated in Theorem 2 is satisfied. □

According to the above theorem, both the reaching phase and the sliding phase satisfy predefined-time stability. Here, $T_{\delta 1}$ adjusts the settling time for the system state to converge from the sliding surface to the origin, and $T_{\delta 2}$ controls the settling time for the system to reach the sliding surface from the initial state. Consequently, the manipulator system's total convergence time is bounded by $T_\delta \leq T_{\delta 1} + T'_{\delta 2} + T'_d$. The control structure diagram of the manipulator system is shown in Figure 3.

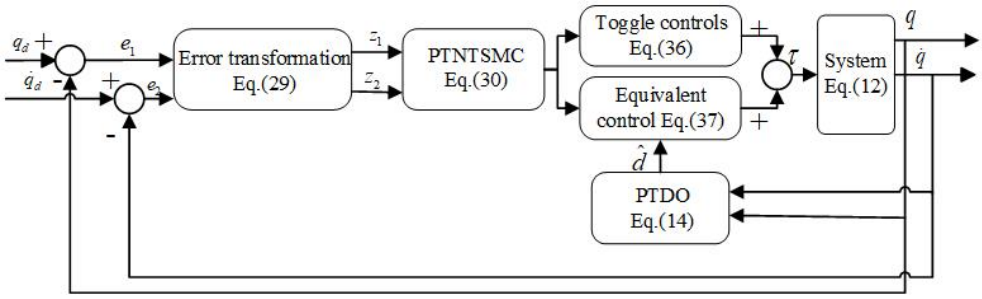


**Figure 3.** Control block diagram of the manipulator system.

## 4. Simulation Verification

### *4.1. Simulation Parameter Settings*

To validate the effectiveness and robustness of the proposed control algorithm, simulation experiments are conducted based on the established dynamic model. The proposed control method is compared with controllers from different references. The two-degree-of-freedom structure is illustrated in Figure 4.

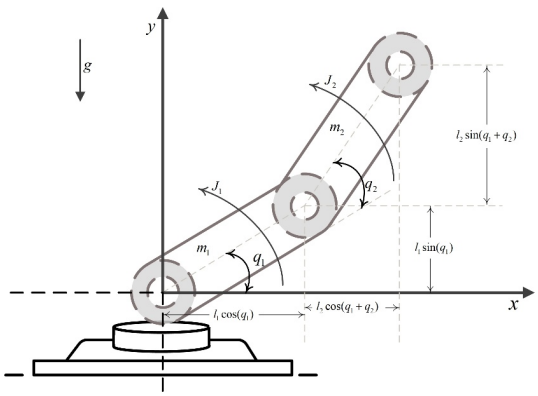

**Figure 4.** Dynamic model of the manipulator.

A numerical validation of the proposed control strategy is carried out on a two-degree-of-freedom robotic manipulator. The system dynamics are characterized by joint angular positions $q_1, q_2$ and their corresponding velocities $\dot{q}_1, \dot{q}_2$. The mechanical parameters include link lengths $l_1, l_2$ and moments of inertia $J_1, J_2$. The dynamic matrices $M(q)$, $C(q, \dot{q})$, and $G(q)$ referenced in Equation (50) are explicitly defined as follows:

$$M(q) = \begin{bmatrix} m_{11} & m_{12} \\ m_{21} & m_{22} \end{bmatrix}, \qquad C(q, \dot{q}) = \begin{bmatrix} c_{11} & c_{12} \\ c_{21} & c_{22} \end{bmatrix}, \tag{49}$$

$$G(q) = \begin{bmatrix} (m_1 + m_2) l_1 g \cos q_1 + m_2 l_2 g \cos(q_1 + q_2) \\ m_2 l_2 g \cos(q_1 + q_2) \end{bmatrix}, \tag{50}$$

the components of $M(q)$ and $C(q,\dot{q})$ are given by

$$\begin{cases} m_{11} = (m_1 + m_2)l_1^2 + m_2 l_2^2 + 2m_2 l_1 l_2 \cos q_2 + J_1, \\ m_{12} = m_2 l_2^2 + m_2 l_1 l_2 \cos q_2, \\ m_{21} = m_2 l_2^2 + m_2 l_1 l_2 \cos q_2, \\ m_{22} = m_2 l_2^2 + J_2, \\ c_{11} = -m_2 l_1 l_2 \sin(q_2)\dot{q}_1^2, \\ c_{12} = -m_2 l_1 l_2 \sin(q_2)(\dot{q}_1 + \dot{q}_2), \\ c_{21} = m_2 l_1 l_2 \sin(q_2)\dot{q}_1, \\ c_{22} = 0, \end{cases} \tag{51}$$

the manipulator parameters in Equations (50) and (51) are listed in Table 1.

**Table 1.** Parameters of the manipulator.

| Symbol | Value | Symbol | Value | Symbol | Value |
|---|---|---|---|---|---|
| $m_1$ | 0.5 kg | $l_1$ | 1 m | $J_1$ | 0.2 kg · m$^2$ |
| $m_2$ | 1.5 kg | $l_2$ | 0.8 m | $J_2$ | 0.35 kg · m$^2$ |
| $g$ | 9.8 m/s$^2$ | | | | |

The initial joint positions of the manipulator are set to $q = [0.3, -0.3]^{\mathrm{T}}$, initial angular velocities $\dot{q} = [0, 0]^{\mathrm{T}}$, and the desired joint trajectories are selected as $q_d = [\sin 3t, 0.5 \sin 4t]^{\mathrm{T}}$. Model uncertainties are $\Delta M(q) = 0.2M(q)$, $\Delta C(q,\dot{q}) = 0.2C(q,\dot{q})$, $\Delta G(q) = 0.2G(q)$, and the external disturbance signal is $\tau_d = [3 \sin 0.5t, 2 \cos 0.6t]^{\mathrm{T}}$. Predefined-time controller parameters: $\eta_1 = 0.6$, $\eta_2 = 0.6$, $\beta = 0.5$, $\theta = 70$, $\zeta_1 = \zeta_2 = 4$, $K = 8.5$. Prescribed performance constraint parameters: $\rho_1 = 0.8$, $\rho_2 = 0.8$, $\lambda_0 = 1.0$, $\lambda_\infty = 0.05$, $\kappa = 3$. Disturbance observer parameters: $\eta = 0.6$, $\zeta = 1.2$, $T_d = 0.5$, $\beta_d = 5$.

### *4.2. Performance Under Different Predefined Times*

Simulations are carried out using four sets of predefined-time parameters from Table 2 to verify the proposed controller's predefined-time convergence features. The results are displayed in Figures 5 and 6.

**Table 2.** Predefined time constraint parameters.

| Parameter | Group 1 | Group 2 | Group 3 | Group 4 |
|---|---|---|---|---|
| $T_{\delta_1}$ | 0.5 s | 0.7 s | 0.4 s | 0.6 s |
| $T_{\delta_2}$ | 0.3 s | 0.5 s | 0.2 s | 0.4 s |
| $T_{\bar{\delta}}$ | 0.8 s | 1.2 s | 0.6 s | 1.0 s |

Figures 5 and 6 show the tracking errors and control torques of the two joints under different predefined-time parameters. The results indicate that both joints achieve fast and accurate trajectory tracking; the tracking error is always confined within the prescribed performance boundary and converges to a small neighborhood near the origin within the given predefined time. Smaller predefined-time parameters lead to faster error convergence. Although selecting smaller predefined-time parameters helps improve transient performance, the peak input torque of the manipulator also increases. Therefore, a reasonable trade-off between the choice of predefined time and control torque is necessary while ensuring transient performance.

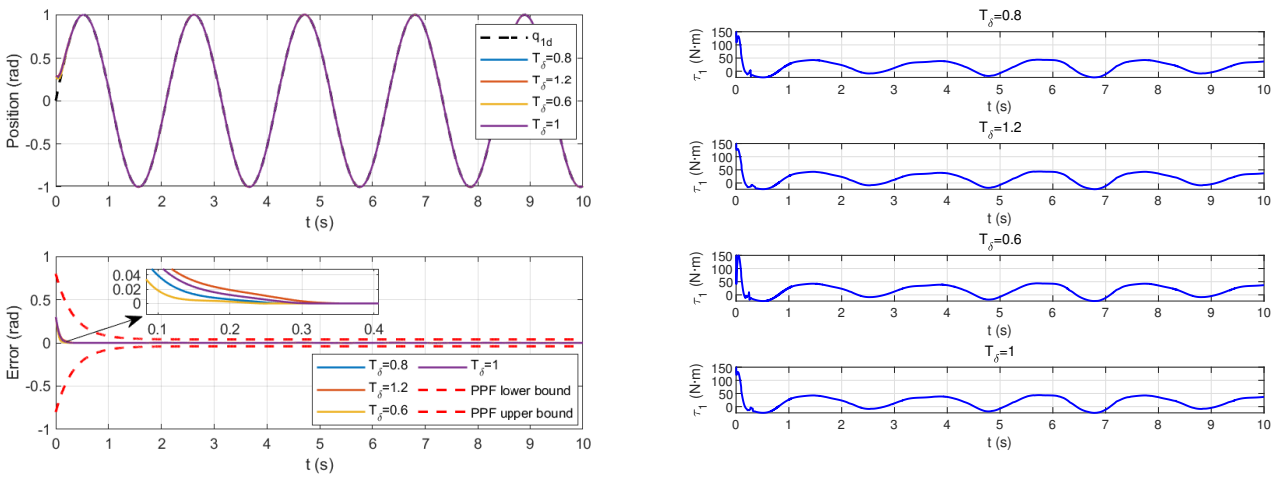


(**a**) (**b**)

**Figure 5.** Joint 1 trajectory tracking, tracking error, and control torque under different predefined-time settings. (**a**) Tracking and error of joint trajectory for joint 1; (**b**) Control torque of joint 1.

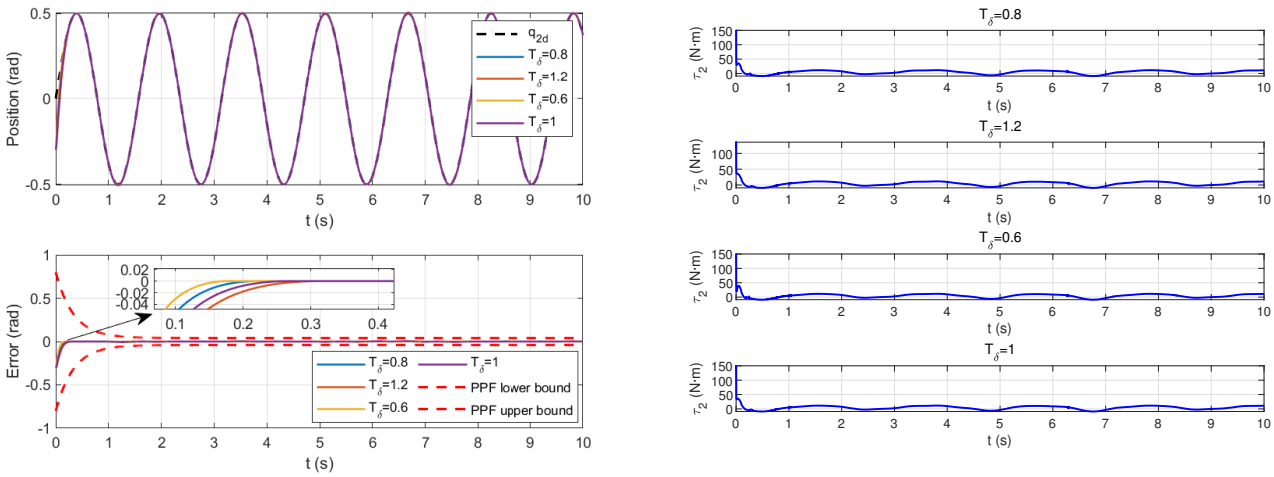


(**a**) (**b**)

**Figure 6.** Joint 2 trajectory tracking, tracking error, and control torque under different predefined-time settings. (**a**) Tracking and error of joint trajectory for joint 2; (**b**) Control torque of joint 2.

### *4.3. Performance Under Different Initial Conditions*

To verify the predefined-time tracking performance under the same desired trajectory and the same predefined-time control but different initial conditions, the specific initial conditions are listed in Table 3.

**Table 3.** Initial state parameters.

| Condition | $q_1(0)$ | $\dot{q}_1(0)$ | $q_2(0)$ | $\dot{q}_2(0)$ |
|---|---|---|---|---|
| Case 1 | 0.30 | 0 | −0.30 | 0 |
| Case 2 | 0.52 | 0 | −0.50 | 0 |
| Case 3 | −0.25 | 0 | 0.60 | 0 |
| Case 4 | −0.34 | 0 | 0.30 | 0 |

Figures 7 and 8 show the position tracking responses and error evolution curves of the two-joint manipulator under multiple sets of different initial conditions. The simulation results demonstrate that even with significant initial position deviations, the system can quickly track the desired trajectory; the error remains strictly inside the prescribed performance bound and achieves convergence by the predefined time. The convergence rate is almost unaffected by the magnitude of the initial error, directly verifying the theoretical property that the upper bound of the convergence time in predefined-time control is independent of the initial state, ensuring fast and stable tracking under arbitrary initial deviations.

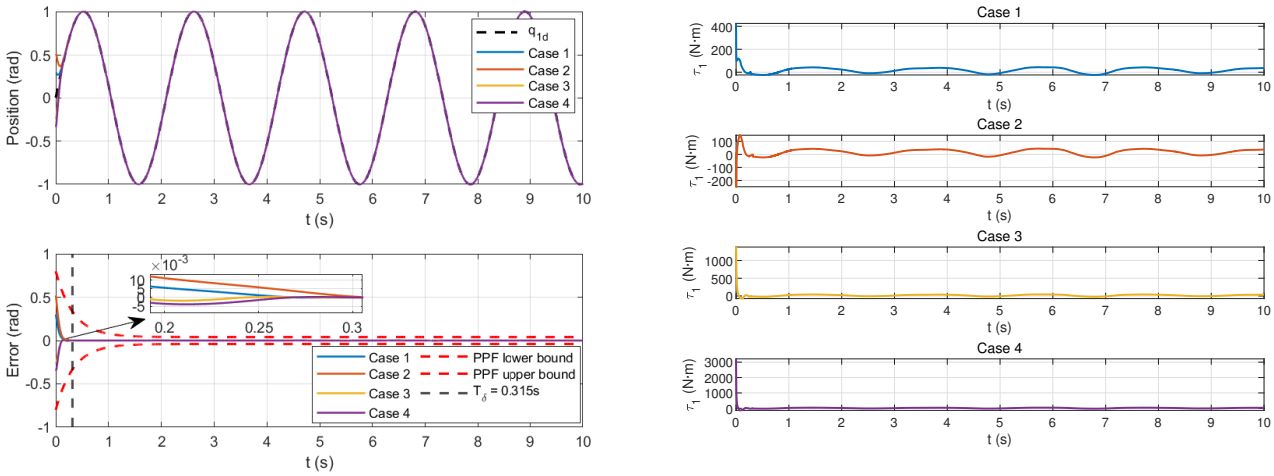


(**a**) (**b**)

**Figure 7.** Joint 1 tracking response, error and control torque under different initial conditions. (**a**) Tracking response and error; (**b**) control torque.

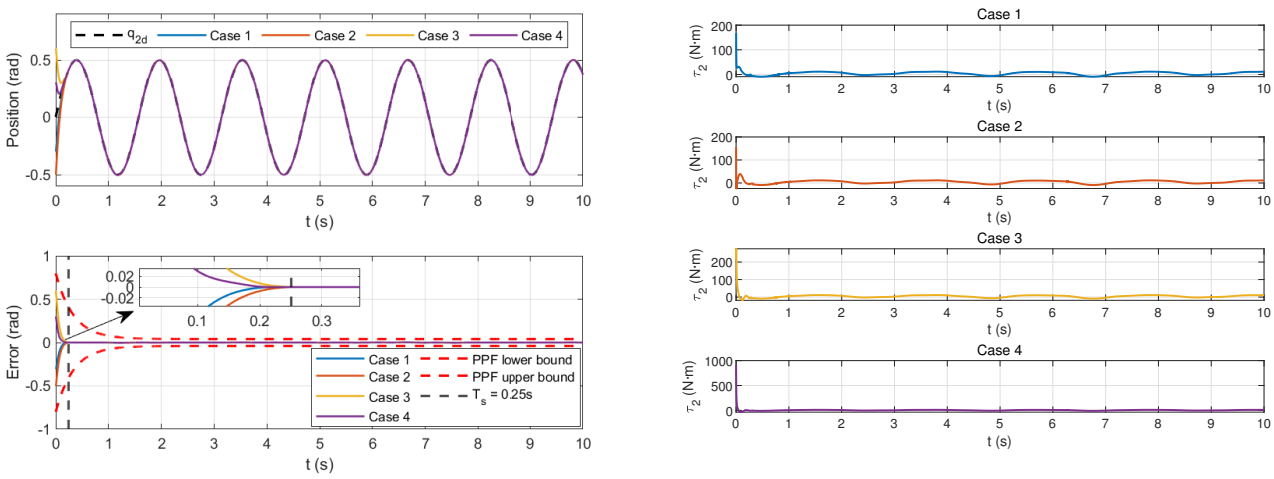


(**a**) (**b**)

**Figure 8.** Joint 2 tracking response, error and control torque under different initial conditions. (**a**) Tracking response and error; (**b**) control torque.

### *4.4. Influence of the Hyperbolic Tangent Parameter θ*

To quantitatively evaluate the trade-off between chattering suppression and tracking accuracy, three performance metrics are adopted: the integral absolute error (IAE) defined as $\text{IAE} = \int_0^T |z_i(t)|\,dt$, the root mean square error (RMSE) defined as $\text{RMSE} = \sqrt{\frac{1}{N}\sum_{k=1}^{N} z_i^2(k)}$, and the total variation (TV) for torque smoothness defined as $\text{TV} = \sum_{k=1}^{N-1} |\tau(k+1) - \tau(k)|$, where $z_i(t)$ is the tracking error of the $i$-th joint, $z_i(k)$ and $\tau(k)$ are the error and torque

at the $k$-th sampling instant, and $N$ is the total number of samples. These metrics are employed to compare the proposed controller under different values of $\theta$ (see Figure 9), and the numerical results are summarized in Table 4.

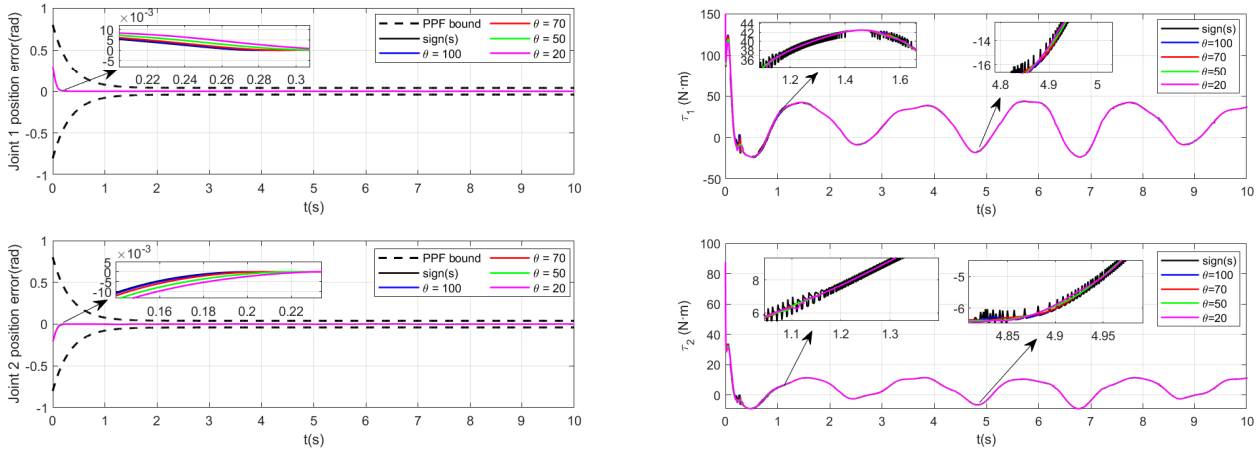


(**a**) (**b**)

**Figure 9.** Tracking error and control torque responses under different $\theta$ values. (**a**) Tracking error of joint 1 and joint 2; (**b**) Control torque of joint 1 and joint 2.

**Table 4.** Quantitative Comparison of Tracking Accuracy and Torque Smoothness under Different $\theta$ Values.

| | RMSE1 | RMSE2 | IAE1 | IAE2 | TV1 | TV2 |
|---|---|---|---|---|---|---|
| $\mathrm{sign}(s)$ | 0.016483 | 0.012659 | 0.0178 | 0.0166 | 2788.08 | 921.15 |
| $\theta = 100$ | 0.016484 | 0.012667 | 0.0179 | 0.0167 | 932.48 | 354.24 |
| $\theta = 70$ | 0.016489 | 0.012695 | 0.0182 | 0.0171 | 829.88 | 314.45 |
| $\theta = 50$ | 0.016510 | 0.012777 | 0.0192 | 0.0183 | 763.50 | 296.53 |
| $\theta = 20$ | 0.016553 | 0.012900 | 0.0204 | 0.0199 | 752.69 | 296.12 |

From Figure 9 and Table 4, the hyperbolic tangent function $\tanh(\theta s)$ effectively smooths the switching action compared with the original sign function while maintaining nearly unchanged tracking accuracy. Compared with the sign function, the torque total variation decreases significantly even for a relatively small $\theta$. For example, when $\theta = 20$, TV1 decreases from 2788.08 to 752.69, corresponding to a reduction of 73%. As $\theta$ increases, $\tanh(\theta s)$ gradually approaches the sign function, resulting in only marginal changes in RMSE and IAE, but a noticeable increase in torque variation and hence a stronger chattering tendency. Therefore, a clear trade-off exists between tracking accuracy and chattering suppression. In practical applications, $\theta$ can be tuned according to the desired balance between torque smoothness and tracking performance. In this study, $\theta = 70$ is adopted as a compromise setting for the subsequent simulations. A similar trend is also observed for Joint 2.

### *4.5. Observer Performance Analysis*

Figure 10 verifies the effectiveness of the observer from two aspects: disturbance estimation and control performance. As shown in Figure 10a, the estimated disturbances for both joints closely track the actual lumped disturbances after a short transient. To quantitatively evaluate the influence of observer compensation on tracking performance, three standard error indices are adopted: the IAE, the ISE, and the RMSE. Figure 10b and Table 5 show that observer compensation significantly improves the tracking performance of both joints. For Joint 1, the IAE, ISE, and RMSE are reduced by 71.63%, 12.95%, and 6.60%,

respectively, while for Joint 2, the corresponding reductions are 79.24%, 35.57%, and 19.55%. These results quantitatively confirm the effectiveness of the proposed disturbance observer in improving disturbance rejection and tracking accuracy.

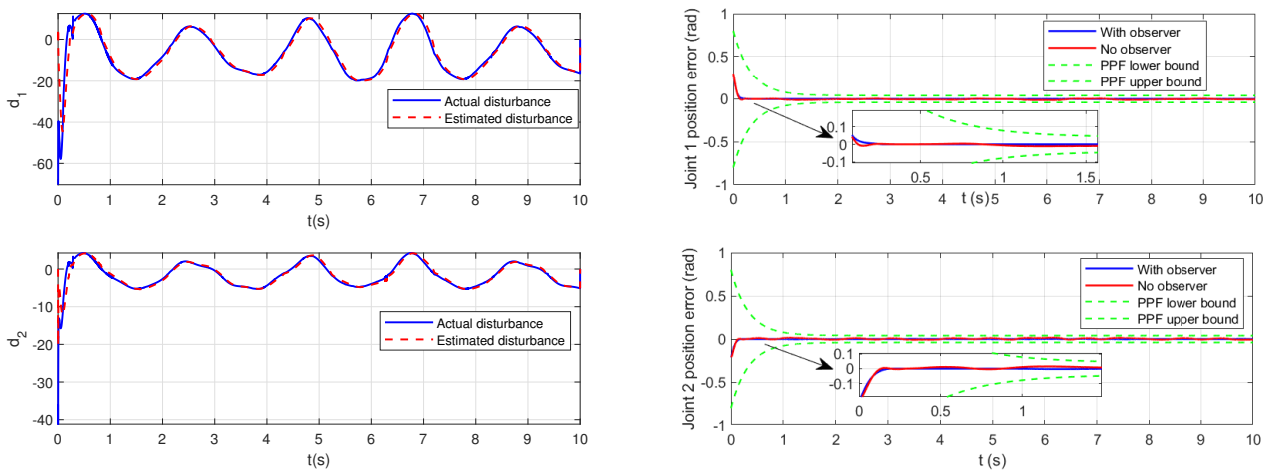


(**a**) (**b**)

**Figure 10.** Interference estimation and tracking error performance of two joints. (**a**) Disturbance and its estimation; (**b**) Joint tracking error with or without observer compensation.

**Table 5.** Quantitative tracking performance comparison with/without observer compensation.

| | Joint 1 | | | Joint 2 | | |
|---|---|---|---|---|---|---|
| | **IAE** | **ISE** | **RMSE** | **IAE** | **ISE** | **RMSE** |
| With observer | 0.017852 | 0.002672 | 0.016484 | 0.016691 | 0.001585 | 0.012667 |
| Without observer | 0.062931 | 0.003070 | 0.017649 | 0.080395 | 0.002459 | 0.015746 |

### *4.6. Controller Comparison Analysis*

To verify the performance of the proposed control algorithm, we compare it against the fixed-time nonsingular fast terminal sliding mode control (FNFTSMC) presented in [14] and the finite-time nonsingular fast terminal sliding mode control (NFTSMC) from [8]. To ensure fairness, the same prescribed performance function and predefined-time observer are used. The comparison is conducted from the perspectives of control accuracy, settling time, and controller output performance.

The fixed-time nonsingular fast terminal sliding mode surface and control law are designed as

$$\begin{cases} s = z_2 + \alpha|z_1|^{\alpha_1}\mathrm{sgn}(z_1) + \beta|z_1|^{\alpha_2}\mathrm{sgn}(z_1), \\ \tau_{\mathrm{eq}} = M_0(\ddot{q}_d - H\dot{e} - \dot{H}e) + C_0\dot{q} + G_0 - \hat{d} - M_0P^{-1}\Big(\dot{P}(\dot{e} + He) + \alpha\alpha_1|z_1|^{\alpha_1-1}z_2 \\ \quad + \beta\alpha_2|z_1|^{\alpha_2-1}z_2\Big), \\ \tau_{\mathrm{sw}} = -M_0P^{-1}\Big(\big(k_1\|s\|^{\phi} + k_2\|s\|^{-\phi}\big)s\Big), \end{cases} \tag{52}$$

where $\alpha_1 = 1 + \phi/2$, $\alpha_2 = 1 - \phi/2$, $0 < \phi < 1$, $k_1 = \alpha\gamma^{1+\phi/2}$, $k_2 = \beta\gamma^{1-\phi/2}$, $\gamma$ is an auxiliary parameter. The controller parameters are set to $\alpha = 11.5$, $\beta = 3$, $\phi = 0.12$, $\gamma = 2$.

The finite-time nonsingular terminal sliding mode surface and control law are designed as

$$\begin{cases} s = z_2 + k_1|z_1|^{\alpha_1}\mathrm{sgn}(z_1) + k_2|z_1|^{\alpha_2}\mathrm{sgn}(z_1), \\ \tau_{\mathrm{eq}} = M_0(\ddot{q}_d - H\dot{e} - \dot{H}e) + C_0\dot{q} + G_0 - \hat{d} - M_0P^{-1}\Big(\dot{P}(\dot{e} + He) + k_1\alpha_1|z_1|^{\alpha_1-1}z_2 \\ \quad + k_2\alpha_2|z_1|^{\alpha_2-1}z_2\Big), \\ \tau_{\mathrm{sw}} = -M_0P^{-1}\big(k_{1\mathrm{sw}}s + k_{2\mathrm{sw}}\mathrm{sat}(s/\phi)\big), \end{cases} \tag{53}$$

where $0 < \alpha_2 < 1$, $\alpha_1 > \alpha_2$, $\mathrm{sat}(\cdot)$ is the saturation function. The NTSMC controller parameters in this paper are set to $k_1 = 4$, $k_2 = 4$, $\alpha_1 = 2$, $\alpha_2 = 0.6$, $k_{1\mathrm{sw}} = 5.0$, $k_{2\mathrm{sw}} = 2.0$, and the saturation boundary layer thickness $\phi = 0.2$.

For a more intuitive comparison of the three controllers, four error evaluation metrics are adopted under the same initial conditions: Integral Absolute Error (IAE) $\mathrm{IAE} = \int_0^T |z_i(t)|\,dt$, Integral Time-weighted Absolute Error (ITAE) $\mathrm{ITAE} = \int_0^T t|z_i(t)|\,dt$, Integral Squared Error (ISE) $\mathrm{ISE} = \int_0^T z_i^2(t)\,dt$, and Root Mean Square Error (RMSE) $\mathrm{RMSE} = \sqrt{\frac{1}{n}\sum_{i=1}^n z_i^2}$. In addition, the total control energy (TCE) defined as $\mathrm{TCE} = \int_0^T |\tau(t)|\,dt$ is introduced to evaluate control effort. These metrics effectively quantify the system control performance, and the specific results are shown in Tables 4 and 5.

Figures 11 and 12 and Tables 6 and 7 present a comparison of the position tracking errors, control torques, and quantitative performance metrics for the two joints under the three control schemes. All three schemes achieve desired trajectory tracking, but with notable quantitative differences. For Joint 1, compared to FNFTSMC, the proposed PTNTSMC reduces IAE by 54.3%, ITAE by 86.8%, ISE by 20.6%, and RMSE by 11.3%; compared to NFTSMC, the reductions are 89.0%, 98.5%, 54.2%, and 32.4%, respectively. For Joint 2, PTNTSMC outperforms FNFTSMC with reductions of 63.1% (IAE), 79.3% (ITAE), 52.9% (ISE), and 31.7% (RMSE); relative to NFTSMC, the improvements are 93.3%, 97.6%, 90.8%, and 69.6%, respectively. The tracking error of PTNTSMC converges within 0.3–0.5 s, which is significantly faster than the benchmark methods, while strictly respecting the prescribed performance boundary. The control torque curves show that PTNTSMC and FNFTSMC have smooth inputs without chattering, while NFTSMC exhibits significant peak fluctuations. In addition to the tracking-error indices, the total control energy (TCE) is compared; the proposed PTNTSMC achieves the lowest TCE for both joints, indicating that its superior tracking performance does not come at the expense of higher control effort. These quantitative results clearly demonstrate the superiority of the proposed scheme in error suppression, convergence speed, tracking accuracy, and energy efficiency.

**Table 6.** Comparison of tracking indices and total control energy for joint 1.

| | **PTNTSMC** | **FNFTSMC** | **NFTSMC** |
|---|---|---|---|
| IAE | 0.0179 | 0.0392 | 0.1623 |
| ITAE | 0.0113 | 0.0855 | 0.7704 |
| ISE | 0.0027 | 0.0034 | 0.0059 |
| RMSE | 0.0165 | 0.0186 | 0.0244 |
| TCE | 237.6831 | 238.7379 | 247.1368 |

**Table 7.** Comparison of tracking indices and total control energy for joint 2.

| | **PTNTSMC** | **FNFTSMC** | **NFTSMC** |
|---|---|---|---|
| IAE | 0.0167 | 0.0452 | 0.2488 |
| ITAE | 0.0221 | 0.1066 | 0.9390 |
| ISE | 0.0016 | 0.0034 | 0.0174 |
| RMSE | 0.0127 | 0.0186 | 0.0418 |
| TCE | 65.0177 | 66.3448 | 67.2005 |

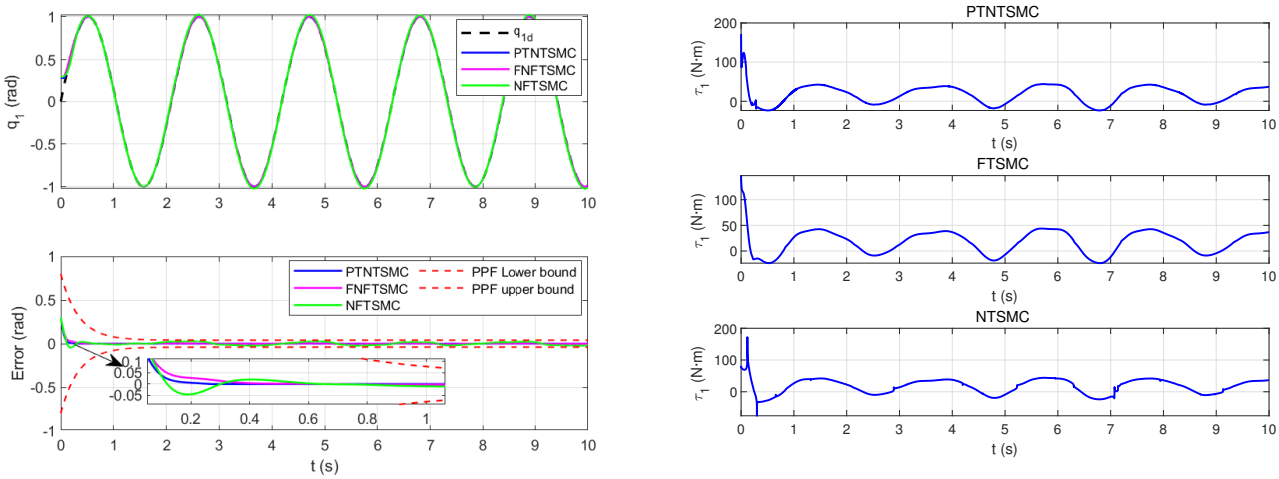


(**a**) (**b**)

**Figure 11.** Performance comparison of joint 1 under different control schemes. (**a**) Position tracking response and tracking error; (**b**) Control torque.

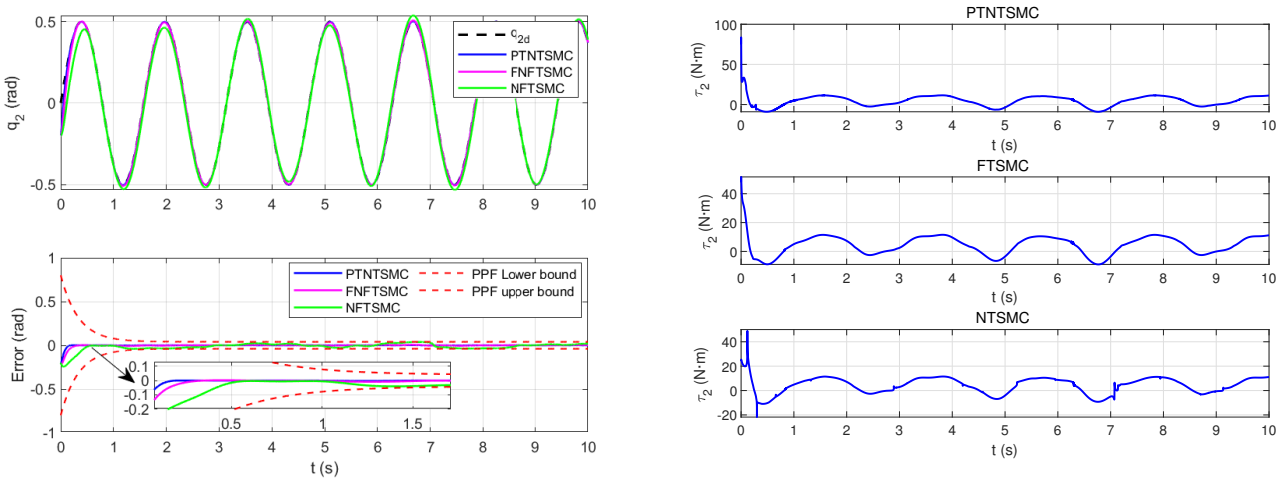


(**a**) (**b**)

**Figure 12.** Performance comparison of joint 2 under different control schemes. (**a**) Position tracking response and tracking error; (**b**) Control torque.

## 5. Conclusions

To address the trajectory tracking problem of a manipulator under model uncertainties and external disturbances, we develop a nonsingular sliding mode control method that combines a PTNDO and prescribed performance. The theoretical and simulation results show that the disturbance observer can accurately estimate the lumped disturbance within the set time limit, and the observation error is uniformly bounded. By introducing a prescribed performance function to transform the error, the error is restricted to a given bound, which guarantees the transient and steady-state behavior of the system. A PTNTSM surface is built to make the system state converge rapidly; with the help of saturation function and hyperbolic tangent function, the control singularity problem is eliminated, chattering is suppressed, and the stable control quantity is output. The overall convergence time of the system is not affected by the initial state, and the relevant parameters can be flexibly adjusted according to the actual working conditions. Compared with the finite time and fixed time sliding mode control algorithm, the proposed strategy has

faster convergence, higher tracking accuracy, stronger anti-interference and initial state adaptation ability, and can meet the requirements of high-precision trajectory tracking in the disturbance environment. In the future, the applicable scenarios of the algorithm will be expanded, and the adaptive performance adjustment strategy will be studied to adapt to the actual engineering constraints such as input saturation.

**Author Contributions:** Conceptualization, S.Y. and Y.W.; methodology, S.Y. and Y.W.; software, Y.W. and Y.Y.; validation, Y.W. and G.S.; formal analysis, Y.W. and G.S.; investigation, Y.W. and Y.Y.; resources, S.Y. and Y.W.; data curation, Y.W.; writing—original draft preparation, Y.W.; writing—review and editing, S.Y. and Y.W.; visualization, S.Y. and Y.W.; supervision, S.Y.; project administration, S.Y.; funding acquisition, G.S. All authors have read and agreed to the published version of the manuscript.

**Funding:** This research was funded by National Natural Science Foundation of China, under grant number 61703224, and the National Natural Science Foundation of China, under grant number 61640302.

**Data Availability Statement:** The original contributions presented in this study are included in the article. For further inquiries, please contact the corresponding author.

**Conflicts of Interest:** The authors declare no conflicts of interest.

## Abbreviations

The following abbreviations are used in this manuscript:

| | |
|---|---|
| PPF | Preset Performance Function |
| PTNDO | Predefined-Time Nonlinear Disturbance Observer |
| PTNTSMC | Predefined-Time Nonsingular Terminal Sliding Mode control |
| FNFTSMC | Fixed-Time Nonsingular Fast Terminal Sliding Mode Control |
| NFTSMC | Finite-Time Nonsingular Fast Terminal Sliding Mode Control |

## References

1. Luo, H.T.; Zhao, F.Q.; Guo, S.W.; Yu, C.S.; Liu, G.M.; Wu, T.K. Mechanical performance research of friction stir welding robot for aerospace applications. *Int. J. Adv. Robot. Syst.* **2021**, *18*, 1729881421996543. [CrossRef]
2. Kim, J.H.; de Mathelin, M.; Ikuta, K.; Kwon, D.S. Advancement of flexible robot technologies for endoluminal surgeries. *Proc. IEEE* **2022**, *110*, 909–931. [CrossRef]
3. Song, L.; Zhu, H.; Zhou, Y.; He, L. Research on operational trajectory control methods and performance testing of multi-degree-of-freedom robotic arms for fruit tree pruning. *Smart Agric. Technol.* **2026**, 102016. [CrossRef]
4. Li, T.L.; Zhang, G.; Zhang, T.; Pan, J. Adaptive neural network tracking control of robotic manipulators based on disturbance observer. *Processes* **2024**, *12*, 499. [CrossRef]
5. Shtessel, Y.; Edwards, C.; Fridman, L.; Levant, A. *Sliding Mode Control and Observation*; Springer: Berlin/Heidelberg, Germany, 2014; Volume 10. [CrossRef]
6. Nguyen, T.B.T.; Truong, H.V.A.; Ahn, K.K. Non-Singular Fast Terminal Sliding Mode Control Based Trajectory Tracking Control of Cable-Driven Manipulators Subject to Lumped Mismatched Uncertainties. *Mathematics* **2026**, *14*, 1602. [CrossRef]
7. Ertugrul, M.; Kaynak, O. Neuro sliding mode control of robotic manipulators. *Mechatronics* **2000**, *10*, 239–263. [CrossRef]
8. Sun, C.C. Robust finite time tracking control for robotic manipulators based on nonsingular fast terminal sliding mode. *Int. J. Control Autom. Syst.* **2022**, *20*, 3285–3295. [CrossRef]
9. Yu, X.H.; Feng, Y.; Man, Z.H. Terminal sliding mode control—An overview. *IEEE Open J. Ind. Electron. Soc.* **2020**, *2*, 36–52. [CrossRef]
10. Andrieu, V.; Praly, L.; Astolfi, A. Homogeneous approximation, recursive observer design, and output feedback. *SIAM J. Control Optim.* **2008**, *47*, 1814–1850. [CrossRef]
11. Polyakov, A. Nonlinear feedback design for fixed-time stabilization of linear control systems. *IEEE Trans. Autom. Control* **2011**, *57*, 2106–2110. [CrossRef]
12. Vo, A.T.; Truong, T.N.; Hong, I.P.; Kang, H.J. Precision tracking of industrial manipulators via adaptive nonsingular fixed-time sliding mode control. *Mathematics* **2025**, *13*, 2641. [CrossRef]

13. Ma, D.S.; Ren, L.; Li, T.L.; Solihin, M.I.; Li, J.C. Fixed-time path tracking control of uncertain robotic manipulator based on adaptive deviation correction and compensation mechanism neural network. *Processes* **2026**, *14*, 278. [CrossRef]
14. Zhu, Z.X.; Huang, M.X.; Wu, Y.Y.; Tan, X.G. Fixed-time sliding mode control for robot manipulators. In Proceedings of the 2024 39th Youth Academic Annual Conference of Chinese Association of Automation (YAC), Dalian, China, 7–9 June 2024; pp. 816–820. [CrossRef]
15. Muñoz-Vázquez, A.J.; Sánchez-Torres, J.D.; Jiménez-Rodríguez, E.; Loukianov, A.G. Predefined-time robust stabilization of robotic manipulators. *IEEE/ASME Trans. Mechatron.* **2019**, *24*, 1033–1040. [CrossRef]
16. Nie, J.; Dong, L.J.; Sun, Q.Q.; Zhang, C.; Zhang, C.Y. Nonsingular predefined-time sliding mode trajectory tracking control for uncertain manipulator with predefined-time extended state observer. *ISA Trans.* **2025**, *167*, 480–502. [CrossRef] [PubMed]
17. Chen, C.Y.; Han, Y.Y.; Zhu, S.; Zeng, Z.G. Distributed fixed-time tracking and containment control for second-order multi-agent systems: A nonsingular sliding-mode control approach. *IEEE Trans. Netw. Sci. Eng.* **2022**, *10*, 687–697. [CrossRef]
18. Wu, C.H.; Yan, J.G.; Shen, J.H.; Wu, X.W.; Xiao, B. Predefined-time attitude stabilization of receiver aircraft in aerial refueling. *IEEE Trans. Circuits Syst. II Express Briefs* **2021**, *68*, 3321–3325. [CrossRef]
19. Wang, F.; Miao, Y.; Li, C.Y.; Hwang, I. Attitude control of rigid spacecraft with predefined-time stability. *J. Frankl. Inst.* **2020**, *357*, 4212–4221. [CrossRef]
20. Chen, Z.Y.; Yang, X.H.; Liu, X.P. RBFNN-based nonsingular fast terminal sliding mode control for robotic manipulators including actuator dynamics. *Neurocomputing* **2019**, *362*, 72–82. [CrossRef]
21. Ni, J.K.; Liu, L.; Liu, C.X.; Hu, X.Y.; Li, S.L. Fast fixed-time nonsingular terminal sliding mode control and its application to chaos suppression in power system. *IEEE Trans. Circuits Syst. II Express Briefs* **2016**, *64*, 151–155. [CrossRef]
22. Bechlioulis, C.P.; Rovithakis, G.A. Robust adaptive control of feedback linearizable MIMO nonlinear systems with prescribed performance. *IEEE Trans. Autom. Control* **2008**, *53*, 2090–2099. [CrossRef]
23. Li, J.; Du, J.L.; Chen, C.L.P. Command-filtered robust adaptive NN control with the prescribed performance for the 3-D trajectory tracking of underactuated AUVs. *IEEE Trans. Neural Netw. Learn. Syst.* **2021**, *33*, 6545–6557. [CrossRef] [PubMed]
24. Wang, Z.C.; Liu, Y. Reduced-order ESO-based fixed-time sliding mode control for robotic manipulator with prescribed performance constraints. *Int. J. Robust Nonlinear Control* **2025**, *35*, 4329–4345. [CrossRef]
25. Tran, M.D.; Kang, H.J. A novel adaptive finite-time tracking control for robotic manipulators using nonsingular terminal sliding mode and RBF neural networks. *Int. J. Precis. Eng. Manuf.* **2016**, *17*, 863–870. [CrossRef]
26. Li, J.X.; Wang, Q.Q.; Fang, Y.M. Adaptive neural network-based practical predefined-time nonsingular terminal sliding mode control for upper limb rehabilitation robots. *Commun. Nonlinear Sci. Numer. Simul.* **2024**, *136*, 108085. [CrossRef]
27. Chen, X.H.; Ding, L.; Wu, W.F.; Wu, H.T. Adaptive neural barrier function-based fast terminal sliding mode control for bionic aerial manipulators in canopy sampling. *Aerospace* **2026**, *13*, 392. [CrossRef]
28. Xu, S.L.; He, B. Robust adaptive fuzzy fault tolerant control of robot manipulators with unknown parameters. *IEEE Trans. Fuzzy Syst.* **2023**, *31*, 3081–3092. [CrossRef]
29. Lu, L.; Liu, W.Q.; Zhang, D.; Cheng, J. Adaptive fixed-time composite learning control of uncertain robotic manipulator systems based on fuzzy system and neural network. *Int. J. Robust Nonlinear Control* **2026**, *36*, 4775–4791. [CrossRef]
30. Yin, S.; Shi, Z.J.; Liu, Y.J.; Xue, G.; You, H.Q. Adaptive non-singular terminal sliding mode trajectory tracking control of robotic manipulators based on disturbance observer under unknown time-varying disturbance. *Processes* **2025**, *13*, 266. [CrossRef]
31. You, H.Q.; Liu, Y.J.; Shi, Z.J.; Wang, Z.K.; Wang, L.; Xue, G. Adaptive non-singular fast terminal sliding mode trajectory tracking control for robotic manipulator with novel configuration based on TD3 deep reinforcement learning and nonlinear disturbance observer. *Sensors* **2026**, *26*, 297. [CrossRef] [PubMed]
32. Liu, Q.Z.; Zhang, L.; Sun, B.; Xiao, Y.; Fan, G.W. Fixed-time disturbance observer-based attitude prescribed performance predictive control for flexible spacecraft. *IEEE Trans. Aerosp. Electron. Syst.* **2024**, *60*, 3209–3220. [CrossRef]
33. Zhang, J.Q.; Yu, S.H. Appointed-fixed-time disturbance observer based nonsingular fixed-time distributed leader-follower formation control for marine surface vessels. *Ocean Eng.* **2026**, *345*, 123725. [CrossRef]
34. Li, T.L.; Zhang, G.; Zhang, T.; Pan, J. Fixed-Time sliding mode control for robotic manipulators based on disturbance observer. *Int. J. Aerosp. Eng.* **2024**, *2024*, 1263459. [CrossRef]
35. Shao, K.; Zheng, J.C. Predefined-time sliding mode control with prescribed convergent region. *IEEE/CAA J. Autom. Sin.* **2022**, *9*, 934–936. [CrossRef]
36. Zeng, X.D.; Hua, C.C.; Li, K. Robust composite adaptive predefined-time control of n-link robotic systems with prescribed performance. *Sci. China Inf. Sci.* **2026**, *69*, 132201. [CrossRef]


**Disclaimer/Publisher's Note:** The statements, opinions and data contained in all publications are solely those of the individual author(s) and contributor(s) and not of MDPI and/or the editor(s). MDPI and/or the editor(s) disclaim responsibility for any injury to people or property resulting from any ideas, methods, instructions or products referred to in the content.